PHOTONICS Research

Cascaded parametric amplification based on spatiotemporal modulations

Qianru Yang,[1,3] Hao Hu,[1] Xiaofeng Li,[2] and Yu Luo[1,*]

[1]School of Electrical and Electronic Engineering, Nanyang Technological University, Singapore 639798, Singapore
[2]School of Optoelectronic Science and Engineering & Collaborative Innovation Center of Suzhou Nano Science and Technology, Soochow University, Suzhou 215006, China
[3]e-mail: qianru002@ntu.edu.sg
*Corresponding author: luoyu@ntu.edu.sg

Received 8 August 2022; revised 12 October 2022; accepted 27 October 2022; posted 27 October 2022 (Doc. ID 472233); published 21 April 2023

Active devices have drawn considerable attention owing to their powerful capabilities to manipulate electromagnetic waves. Fast and periodic modulation of material properties is one of the key obstacles to the practical implementation of active metamaterials and metasurfaces. In this study, to circumvent this limitation, we employ a cascaded phase-matching mechanism to amplify signals through spatiotemporal modulation of permittivity. Our results show that the energy of the amplified fundamental mode can be efficiently transferred to that of the high harmonic components if the spatiotemporal modulation travels at the same speed as the signals. This outstanding benefit enables a low-frequency pump to excite parametric amplification. The realization of cascaded parametric amplification is demonstrated by finite-difference time-domain (FDTD) simulations and analytical calculations based on the Bloch–Floquet theory. We find that the same lasing state can always be excited by an incidence at different harmonic frequencies. The spectral and temporal responses of the space-time modulated slab strongly depend on the modulation length, modulation strength, and modulation velocity. Furthermore, the cascaded parametric oscillators composed of a cavity formed by photonic crystals are presented. The lasing threshold is significantly reduced by the cavity resonance. Finally, the excitation of cascaded parametric amplification relying on the Si-waveguide platform is demonstrated. We believed that the proposed mechanism provides a promising opportunity for the practical implementation of intense amplification and coherent radiation based on active metamaterials.

https://doi.org/10.1364/PRJ.472233

1. INTRODUCTION

Active devices can enable a wealth of advanced functions in photon manipulation, including frequency conversion [1–4], amplification [5–7], and isolation [8–15], which can hardly be achieved by conventional passive devices. Instead of realizing new functions based on established mechanisms, time has merged as a new degree of freedom to control waves [16,17]. The periodic modulation of optical properties in time and space enables photonic interband transition [18], quasi-phase matching for momentum and energy [19], unidirectional amplification [20], dispersion engineering [7,21], and parity-time (PT)-phase transition [6,22]. Several temporal counterparts of the physical effects are unveiled, e.g., Fresnel drag [23], Anderson localization [24], and Wood anomalies [25]. In addition, from the perspective of topology, time modulation enables a new synthetic dimension to excite high-dimensional topological states [26–30].

Despite the thriving development in theory, the realization of fast modulation becomes a formidable challenge that prevents active metamaterials and metasurfaces from being used in practical applications. Many efforts have been made to realize dynamic modulation by new materials and advanced nanofabrication [1,2,8–10,31–34]. The sudden change in the refractive index on the order of the subpicosecond has been realized by photonic excitation [31]. It enables frequency conversion at near-infrared frequencies [1]. However, some applications, e.g., isolation, require the periodic modulation of material properties in space and time simultaneously. The periodic modulation with a frequency ranging from several GHz to THz has been demonstrated based on photoelectric [8], photoacoustic [9,13], and nonlinear Kerr effects [10]. After all, the applications based on dynamic modulation are still hampered by the implementation of fast modulation at infrared and optical frequencies.

Parametric amplification (PA) is an irreplaceable mechanism that is used to generate coherent light at frequencies that are not sustained by the gain media in nature. In the past decades, PA has also revolutionized the generation of isolated attosecond pulses and is promoting the development of strong field physics [35]. Compared with amplifications based on semiconductor and rare-earth-doped media, PA is phase-sensitive and can reduce noise approaching quantum limits by locking the phase between pump and idler waves [36–39]. At present, PA at optical and infrared frequencies relies on second-order or third-order susceptibility of nonlinear materials. Due to the weak nature of nonlinearity, high-intensity and bulky pump sources are usually required, which hinders the integration and miniaturization of devices.

On the other hand, PA can be realized by time modulation. This mechanism is widely used at microwave frequencies. However, it is rarely employed at high frequencies since it requires a modulation frequency comparable to the operating frequency [40,41]. Such a frequency limitation is enforced by the Manley–Rowe relations [42]. To relax the restriction on the modulation frequency, we introduce the spatiotemporal modulation to realize cascaded phase matching between the signal and the amplified fundamental modes at half of the modulation frequency. As shown in Figs. 1(a) and 1(b), the permittivity of the medium is periodically modulated in both space and time. It enables the phase matching of energy and momentum at the same time. Hence, by choosing proper modulation frequencies, efficient cascaded frequency conversion is possible. As a result, a signal with the frequency ω_{inc} much higher than the modulation frequency Ω can be amplified in a cascaded manner [Figs. 1(c) and 1(d)]. This remarkable advantage makes the realization of PA in a time-modulated system possible by using a low-frequency modulation.

In this work, we first show the eigenstate and eigenvalue of space-time modulated media. Second, the realization of cascaded PA is demonstrated by calculating the scattering coefficients of a space-time modulated slab. Next, the lasing nature of cascaded PA and the characteristics of gain mechanisms are analyzed. Finally, the cascaded parametric oscillator and the Si-waveguide-based cascaded PA are presented.

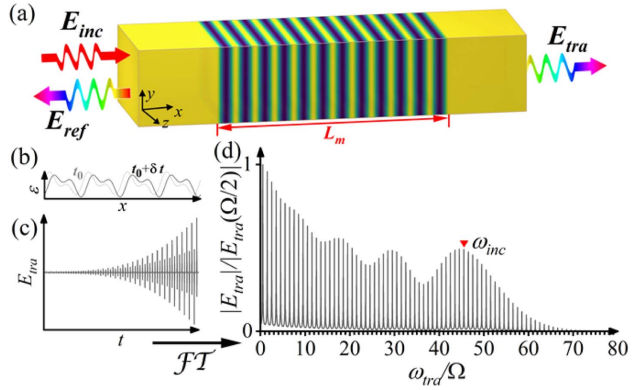

Fig. 1. (a) Schematic of scattering from a space-time modulated slab. (b) The profile of space-time modulated permittivity. (c) The signal can be amplified with time by compensating for the phase mismatching through spatiotemporal modulation. (d) The transmission spectrum. A series of harmonic components with spaced frequency Ω are excited, and the signal is amplified in a cascaded manner.

2. CASCADED PARAMETRIC AMPLIFICATION

A. Cascaded PA Based on Quasi-phase Matching

First, we show PA supported by time-modulated media with permittivity $\varepsilon(t) = \varepsilon_s(1 + 2\alpha \cos \Omega t)$, where α is the modulation strength, Ω is the modulation frequency, ε_s is the background permittivity, and $v_s = (\varepsilon_s \mu_0)^{-1/2}$ is the phase velocity of unmodulated signal waves. The dispersion relation of the time-modulated media is shown in Fig. 2(a). Unlike the traditional photonic crystals, which open bandgaps in the frequency domain, the periodic time modulation forms the inverted bandgaps in the k space. In the inverted bandgaps, eigenfrequencies are complex numbers, and the corresponding eigenstate will be amplified with time, which is the well-known PA. The imaginary part of the eigenfrequency corresponds to the exponential growth rate of the PA and is used for characterizing the parametric gain of the time-modulated system.

From a different perspective, the temporal modulation with pump frequency Ω couples the forward propagating signal and the backward propagating idler at the frequencies of $\Omega/2$ and

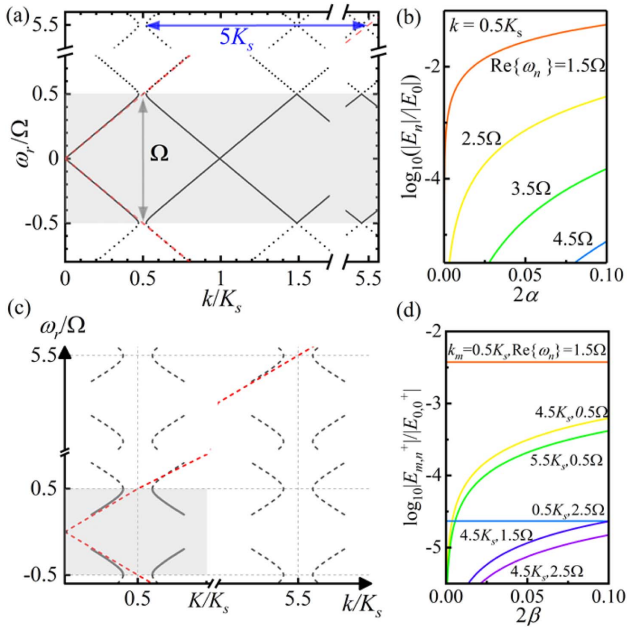

Fig. 2. PA in time-varying media and quasi-phase matching for amplification at the high harmonic frequencies. (a) The dispersion relation of the photonic Floquet media with sinusoidally modulated permittivity $\varepsilon(t) = \varepsilon_s(1 + 2\alpha \cos \Omega t)$, where $\alpha = 0.1$, $\varepsilon_s = 1.46^2\varepsilon_0$, and $K_s = \Omega/v_s$. The shadowed area shows the first Brillouin zone. The red dashed lines indicate the light lines and the blue arrow shows the phase mismatching between the inverted bandgap and the light line. (b) The amplitude of the high harmonic modes as the modulation strength α increases. (c) By introducing spatial modulation with permittivity $\varepsilon(x, t) = \varepsilon_s(1 + 2\alpha \cos \Omega t + 2\beta \cos Kx)$, the inverted bandgaps generate copies of themselves by shifting K. (d) The amplitude of the high harmonic modes as the modulation strength β increases, where $\alpha = 0.01$. Note that the corresponding eigenfrequencies of the eigenstates shown in (b) and (d) are complex numbers.

$-\Omega/2$, respectively [Fig. 2(a)]. The presence of signal waves stimulates the downward frequency conversion leading to the excitation of the idler waves, which in turn amplifies the signal waves through the up-conversion process. Hence, the generation of the signal and idler waves is reinforced by each other, and PA is supported.

As shown in Fig. 2(a), the inverted bandgaps also exist at high harmonic frequencies, e.g., 5.5 Ω, due to the repetition of dispersion relation beyond the first Brillouin zone. However, the magnitude of the electric field at high harmonic frequencies remains small for the modulation strength reaching up to 10% of static permittivity [Fig. 2(b)]. This is because the high harmonic modes are not the allowed modes in the unmodulated media, and their existence relies on the small perturbation. To amplify the signal at a frequency higher than the modulation frequency, the phase mismatching between the amplifying state and the light line needs to be compensated [shown as the blue arrow in Fig. 2(a)].

To compensate for the phase mismatching, we apply spatio-temporal modulation to amplify the signal at the frequency of 5.5Ω. We consider the media with permittivity $\varepsilon(x,t) = \varepsilon_s(1 + 2\alpha \cos \Omega t + 2\beta \cos Kx)$, where $K = 5K_s$. As shown in Fig. 2(c), the inverted bandgaps create copies of themselves by shifting K due to the introduction of spatial modulation. As a result, the inverted bandgap appears near the light line. However, the amplitude of the high harmonic components is still small [Fig. 2(d)]. The reason for the inefficient amplification at the high frequencies can be attributed to the indirect coupling between the fundamental mode and the eigenstates of the unperturbed media. Hence, to increase the amplitude of the harmonic mode at the high frequency, proper spatial and temporal modulation frequencies should be introduced to directly couple the amplifying state and eigenstates near the light line.

B. Cascaded PA Based on Luminal Modulation

In addition to PA, a distinct amplifying process is found to be available by introducing the traveling-wave-like modulation [43]. It has been demonstrated that the number of harmonic components is exponentially increased along the propagation if the modulation velocity equals the phase velocity of the unmodulated signal waves. Such an amplification process, named as luminal amplification (LA), leads to the exponential growth of energy along the propagation [43]. Next, we utilize LA to realize efficient cascaded PA.

Here, we consider a dispersionless space-time modulated medium with permittivity

$$\varepsilon(x,t) = \varepsilon_s[1 + 2\alpha \cos(Kx - \Omega t) + 2\beta \cos \Omega t], \quad (1)$$

where α and β are the modulation strengths. The modulation velocity is defined as $v_m = \Omega/K$. The second term in Eq. (1) represents the luminal modulation if the modulation velocity is within the range $(1 + 2\alpha + 2\beta)^{-1/2} \le v_m/v_s \le (1 - 2\alpha - 2\beta)^{-1/2}$. In this regime, the phase synchronism of all the harmonic components enables efficient frequency conversion in a cascaded manner for sinusoidal modulation. The capability of the efficient frequency conversion is described by the luminal gain in Appendix C. If the luminal gain is comparable with the parametric gain, the energy of the amplified fundamental mode should be efficiently transferred to the harmonic modes at high frequencies.

1. Eigenvalues and Eigenstates

In Fig. 3, we show the eigenfrequencies and eigenstates of media with permittivity described by Eq. (1).

As shown in Fig. 3(a), multiple inverted and normal photonic bandgaps arise. They originate from the coupling between forward and backward propagating waves. As a reference, the dispersion relation of media with $\alpha, \beta \to 0$ is shown as gray solid lines in Fig. 3(a). It satisfies $\omega_{m,n} = \pm v_s k_m$, where (m, n) indicates the order of the harmonic modes, $\omega_{m,n} = \omega + (m+n)\Omega$ is the corresponding harmonic frequency, and $k_m = k + mK$ is the spatial frequency of the harmonic mode. As an example, Table 1 shows the interacting harmonic modes that form the photonic bandgaps. The coupling frequency and wavenumber are denoted as $\Delta\omega$ and Δk, respectively. In general, the inverted (normal) bandgap will be generated if the modulation velocity is

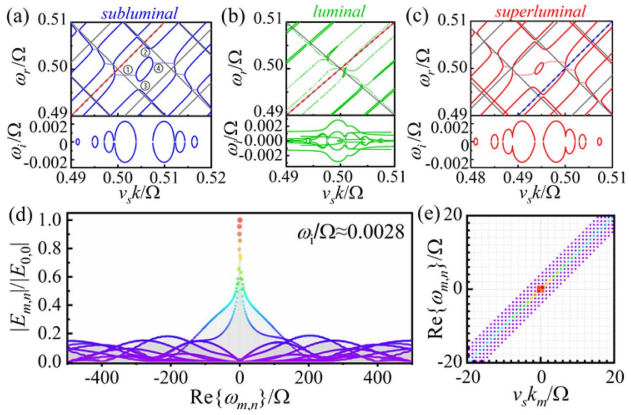

Fig. 3. Eigenvalues and eigenstates of space-time modulated media. The dispersion relation of the space-time modulated media with the modulation velocity in (a) the subluminal regime $[\Omega/K = (1.023\varepsilon_s\mu_0)^{-1/2} < v_s]$, (b) the luminal regime $(\Omega/K = v_s)$, and (c) the superluminal regime $[\Omega/K = (0.978\varepsilon_s\mu_0)^{-1/2} > v_s]$. The permittivity is given by Eq. (1), where $\alpha = \beta = 0.01$. The real and imaginary parts of the eigenfrequencies are depicted in the top and bottom panels, respectively. The colored dots show the real part of the eigenfrequencies in the inverted bandgaps in the top panels. The gray solid lines show the dispersion curves with $\alpha, \beta \to 0$. The red dashed lines in (a) and (b), as well as the blue dashed line in (c), depict the light lines. (d) A typical eigenstate in the inverted bandgap of (b). (e) The corresponding harmonic frequencies and wavenumbers of eigenstate in (d).

Table 1. Type of Photonic Bandgap[a]

No.	Type	(m,n), +[a]	(m,n), −[a]	Δk, $\Delta\omega$
1	Inverted	(0,0)	(0,−1)	0, Ω
2	Normal	(0,0)	(−1,1)	K, 0
3	Normal	(−1,0)	(0,−1)	K, 0
4	Inverted	(−1,0)	(−1,1)	0, Ω

[a] +/− indicates the propagation direction.

$\Delta\omega/\Delta k > v_s$ ($\Delta\omega/\Delta k < v_s$), which corresponds to the superluminal (subluminal) modulation [42,44].

By increasing the modulation velocity from the subluminal regime to the luminal regime, the normal and inverted bandgaps are merged, as shown in Fig. 3(b). To further increase v_m, the bandgaps are separated again [Fig. 3(c)].

The eigenstate of media with $v_m = v_s$ is shown in Fig. 3(d). The amplitude of the high harmonic components is significantly improved. The corresponding wavenumbers are shown in Fig. 3(e). It is found that the amplitude of the harmonic components near the light lines is significantly larger than that of other modes.

2. Scattering from the Slab

To further check the performance of cascaded PA based on luminal modulation, we calculate the transmission from a spatio-temporal modulated slab.

In Fig. 4(a), the magnitudes of the reflection and the transmission coefficients increase with the modulation length. Due to the scattering loss, the system is static when the modulation length L_m is smaller than the threshold length l_c. A similar relationship exists in time-varying media [see Fig. 9(a) in Appendix B].

When $L_m > l_c$, the system is unstable. As shown in Fig. 4(b), the signal at the frequency of 10.5Ω is exponentially amplified after a period of time. To estimate the starting point of lasing, we fit the exponential growth rate of transmission waves. The cross point between the fitted line and static amplitude at the beginning is defined as the critical time for lasing, denoted as t_c. After the critical time point, the amplifying state becomes the dominant one while the static states can be ignored.

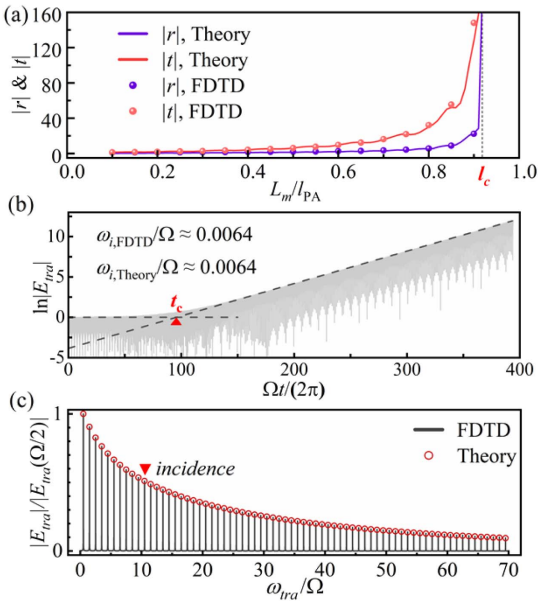

Fig. 4. Cascaded PA supported by a space-time modulated slab. (a) The amplitude of the reflection and the transmission coefficients as the modulation length L_m increases. l_c represents the threshold length of modulation for lasing. Here, $\omega_{inc} = \Omega/2$. (b) The temporal response of the space-time modulated slab with $L_m = 1.1l_{PA} > l_c$ based on FDTD simulations. The critical time point of lasing is estimated by the cross point between the fitted amplified amplitude and the static amplitude before lasing (black dashed lines), denoted as t_c. The numerically fitted and analytically calculated exponential growth rates ω_i are given. (c) The corresponding transmission spectrum. The analytical and numerical results are shown by circles and the solid line, respectively. The incident frequency is equal to 10.5Ω in (b) and (c). The permittivity of the modulated slab is given by Eq. (1) with $K = K_s$, $\alpha = 0.05$, $\beta = 0.1$, and $\varepsilon_s = 1.46^2\varepsilon_0$.

The corresponding transmission spectrum is shown in Fig. 4(c). Since the high harmonic components are amplified by absorbing energy from the fundamental mode, the transmission spectrum is normalized by the amplitude of the electric field at the fundamental frequency, i.e., $E_{tra}(\Omega/2)$, to characterize the luminal gain. A series of harmonic components are amplified at the same time. It demonstrates that the proposed modulation can amplify signals by a low-frequency pump. The proposed modulation for PA can be employed to generate a frequency comb.

We also solved the scattering coefficients of the amplifying state based on the Bloch–Floquet theory. In fact, the lasing state corresponds to a singular state of a space-time modulated slab. Hence, the scattering problem can be solved by an eigenvalue problem without incidence (for more details refer to Appendix A). The numerical and analytical results are in good agreement, as shown in Fig. 4(c).

3. Excitation of Time-growing Mode and Efficient Frequency Conversion

The temporal and the spectral responses of cascaded PA show both characteristics of LA and PA [Figs. 4(b) and 4(c)]. In this section, the gain mechanisms of the cascaded PA through the space-time modulated media are analyzed.

The singular nature of the lasing state implies that the unstable state can be excited by the incidence at any harmonic frequency with non-negligible amplitude in Fig. 4(c). To demonstrate this, we calculate the response of the same modulation excited by an incidence at different harmonic frequencies based on finite-difference time-domain (FDTD) simulation and compare it with the analytical results. As shown in Fig. 5(a), the fitted exponential growth rate based on numerical simulations fluctuates around the theoretical results [see the gray dashed line in Fig. 5(a)]. The corresponding eigenstates are compared in Fig. 5(b). The consistency between numerical and analytical results further proves that the same state is excited. The only difference that is shown in the numerical results [Fig. 5(a)] is that the critical time point of lasing is delayed for input at high harmonic frequencies.

In addition to the modulation strength β, the parametric gain also depends on the modulation length. As shown in Fig. 5(c), the exponential growth rate increases with the modulation length, and the parametric gain tends to be saturated for a lengthened modulation range. The same behavior appears in PA [Fig. 9(c)]. The eigenstate with a larger exponential growth rate can be excited when the scattering loss in the slab is suppressed.

On the other hand, LA behaves as an efficient frequency converter in cascaded PA. As shown in Fig. 5(d), the highest order of frequency conversion in cascaded PA increases with the modulation strength α. The corresponding exponential growth rates ω_i are shown in Fig. 11(a) in Appendix D. We assume that the harmonic components are efficiently amplified if the amplitude is larger than one percent of the magnitude at the fundamental frequency. For $\beta = 0$, the luminal gain can

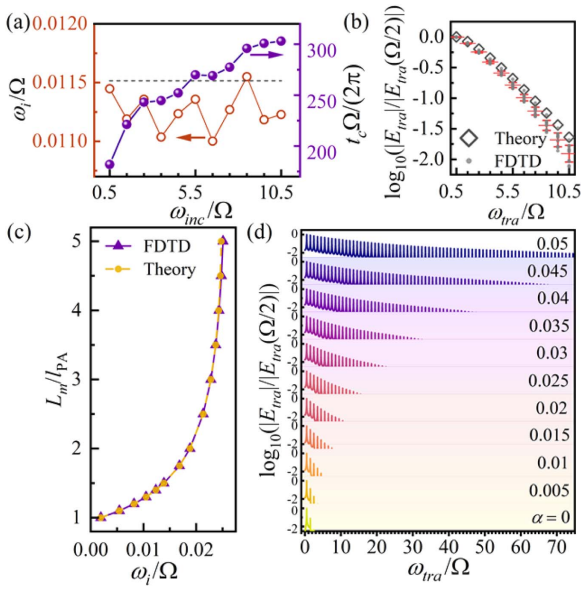

Fig. 5. (a) Exponential growth rate ω_i and critical time point t_c of lasing are calculated by FDTD simulations with the incidence at different frequencies. The dashed line shows the analytically calculated ω_i. (b) The amplitude of the transmission field calculated by the Bloch–Floquet theory (diamonds) and FDTD simulations (light gray dots). The error bars show the mean and the standard deviation of the field amplitude excited by an incidence at different frequencies. (c) The exponential growth rate as the modulation length increases. (d) The highest order of frequency conversion as the modulation strength α increases.

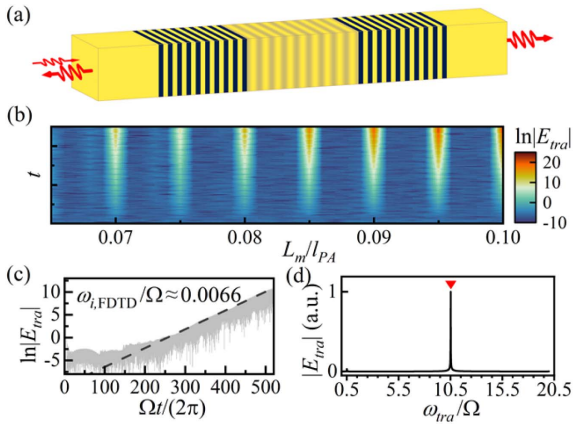

Fig. 6. (a) Schematic of the CPO composed of a space-time modulated slab and a cavity formed by photonic crystals. (b) The temporal response of the space-time modulated slab with varying modulation lengths. Here, $\alpha = \beta = 0.005$ and $K = K_s$. The number of periods is equal to 3 for both PCs on the right and left sides. (c) The temporal response and (d) the transmission spectrum of the CPO operating at a single frequency. The photonic crystal is designed to only allow transmission at the frequency of 10.5Ω. Here, $\alpha = 0.049$, $\beta = 0.05$, $K = 0.95K_s$, and $\varepsilon_s = 3.5^2\varepsilon_0$. The number of periods is equal to 40 for both PCs. For the parameters of the photonic crystals and the band structure see Figs. 12(a) and 12(c) in Appendix E.

be simply evaluated by the exponential relationship between the number of excited harmonic modes and the propagation length (for more details refer to Appendix C). However, for $\beta \neq 0$, the highest order of frequency conversion in cascaded PA does not exponentially increase with propagation [see Fig. 11(b) in Appendix D]. This can be attributed to the coupling with the time-growing state. The highest order of frequency conversion presents the capability to transfer energy from the amplified fundamental mode to high harmonic components, which are different from traditional LA [43].

3. CASCADED PARAMETRIC OSCILLATOR

To reduce the lasing threshold and improve the performance of the amplifier, we design a cascaded parametric oscillator (CPO) composed of a space-time modulated slab and a cavity formed by photonic crystals, as shown in Fig. 6(a). Here, the photonic crystals play a role in high reflection mirrors for all harmonic components. The resonant conditions are satisfied when the phase change of a round trip in the cavity equals $2m\pi$ for $m \in Z$ [see Fig. 12(b) in Appendix E]. The responses of the CPO with the varying length of cavities are presented in Fig. 6(b). It is found that the signal can be amplified when the phase conditions of resonance are fulfilled. The threshold length of lasing is decreased to $0.07l_{\mathrm{PA}}$ and is much smaller than the threshold length of lasing without a cavity.

In addition, we design a CPO operating at a single frequency. The photonic crystals are designed to only allow the transmission at the frequency of 10.5Ω and serve as high reflection mirrors for other harmonic components. The results show that the signal is amplified with time [Fig. 6(c)], and no parasite harmonic modes transmit through the CPO [Fig. 6(d)].

4. Si-WAVEGUIDE-BASED CASCADED PA

Intense amplifiers and light sources at mid-infrared frequencies are extremely desired for the applications of sensing and communications due to the strong characteristic resonances of molecules and the existence of atmospheric transmission windows [45]. Benefiting from the non-dispersive nature of silicon

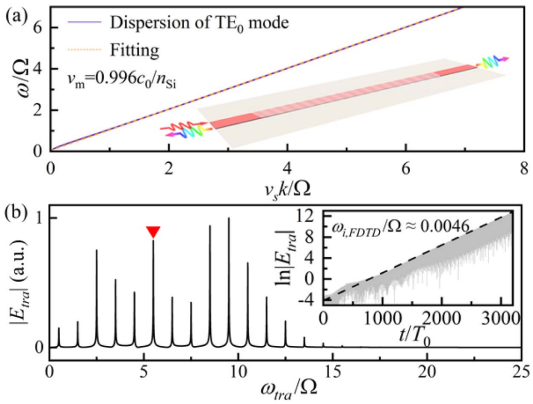

Fig. 7. Cascaded PA based on the Si waveguide. (a) The dispersion relation of an unmodulated Si waveguide with the width of waveguide $d_{\mathrm{WG}} = 2\pi c_0/(n_{\mathrm{Si}}\Omega)$ and the refractive index of Si $n_{\mathrm{Si}} = 3.5$. The fitted velocity of the TE_0 mode is equal to $0.996c_0/n_{\mathrm{Si}}$ and is set as the modulation velocity v_m to achieve cascaded PA. (b) The transmission spectrum of Si waveguide with space-time modulation described by Eq. (1). Here, $\alpha = 0.04$, $\beta = 0.05$, and $L_m = 1.5l_{\mathrm{PA}}$.

beyond ~1100 nm, silicon waveguides become the superior platform to achieve cascaded PA. As shown in Fig. 7(a), the dispersion curve of the TE_0 mode is almost linear. The modulation velocity v_m is set to equal the fitted group velocity of the guided mode to realize cascaded PA.

The signal at the frequency of 5.5Ω can be amplified by imposing spatiotemporal modulation given by Eq. (1), as shown in the inset of Fig. 7(b). The results show that cascaded PA is immune to the moderate dispersion of the guided mode. The spectrum of the transmission field is presented in Fig. 7(b).

5. CONCLUSION

In summary, we reported that PA can be achieved in a spatiotemporal modulated medium with a modulation frequency much lower than the oscillation frequency of electromagnetic waves. Benefitting from the strong interaction between harmonic modes based on luminal modulation, it has been demonstrated that the energy can be efficiently transferred from the amplified fundamental mode to the signal in a cascading manner. It is found that the lasing state cannot be excited if the parametric gain is unable to compensate for the scattering loss. Based on the characteristics of PA and LA, we presented that the parametric gain can be evaluated by the exponential growth rate of the amplifying state, and the luminal gain can be assessed through the efficiency of harmonic conversion from the amplified fundamental mode. Furthermore, we have shown that the threshold of cascaded PA can be significantly reduced by introducing a cavity resonating at all harmonic frequencies. Finally, realistic implementation of cascaded PA based on a Si waveguide is proposed. We show that the cascaded PA is immune to the moderate dispersion of the guided mode. Our design not only provides a practical solution for amplification and radiation based on spatiotemporal modulation at infrared and optical frequencies but also opens up a new opportunity to control, for example, spontaneous emission [46–49].

APPENDIX A: BLOCH–FLOQUET THEORY TO SOLVE SCATTERING COEFFICIENTS OF A SPACE-TIME MODULATED SLAB

In this section, we solve the eigenvalues and eigenstates of media with permittivity described by Eq. (1). For normal incidence, the electric and magnetic fields should satisfy Maxwell's equations given by

$$\frac{\partial E_z}{\partial x} = \mu_0 \frac{\partial H_y}{\partial t}, \tag{A1a}$$

$$\frac{\partial H_y}{\partial x} = \frac{\partial \varepsilon(x,t) E_z}{\partial t}. \tag{A1b}$$

Due to the periodicity of permittivity in space and time, the ansatz of Maxwell's equations can take the Bloch–Floquet form

$$E_z(x,t) = \sum_{m,\,n=-\infty}^{+\infty} E_{m,n} e^{ik_m x - i\omega_{m,n} t}, \tag{A2a}$$

$$H_y(x,t) = \sum_{m,\,n=-\infty}^{+\infty} H_{m,n} e^{ik_m x - i\omega_{m,n} t}, \tag{A2b}$$

where the harmonic frequency $\omega_{m,n} = \omega + (m+n)\Omega$ and the wavenumber $k_m = k + mK$ for $m, n \in Z$. By inserting the ansatz into Maxwell's equations, the eigenvalue k or ω and eigenstates $[E_{m,n}, H_{m,n}]^T$ can be solved through

$$\begin{cases} k_m E_{m,n} = -c_0^{-1} \omega_{m,n} \tilde{H}_{m,n} \\ k_m \tilde{H}_{m,n} = -\varepsilon_{r,s} c_0^{-1} \omega_{m,n} (E_{m,n} + \alpha E_{m-1,n} + \alpha E_{m+1,n} + \beta E_{m,n-1} + \beta E_{m,n+1}) \end{cases}, \tag{A3}$$

where $\tilde{H}_{m,n} = z_0 H_{m,n}$, and $z_0 = (\mu_0/\varepsilon_0)^{1/2}$ is the free space impedance.

Note that the negative harmonic frequencies are included in the calculations. In fact, the same state exists with positive frequency. If we consider two states with real wavenumbers $k_1 = -k_2$ and complex eigenfrequencies $\omega_1 = -\omega_2^*$, then the corresponding eigenstates have a relationship $E_{m,n}^{(1)} = (E_{m,n}^{(2)})^*$, which can be verified by Eq. (A3). Hence, they are in the same state located at the first and third quadrants or second and fourth quadrants of the $k - \omega$ plane based on the complex exponential form of ansatz.

Since the high degeneracy of harmonic components is in the luminal regime, the Bloch–Floquet description of the solution fails for finite terms of expansion in practical calculation, and the eigenvalue problem will not converge [42]. However, for a space-time modulated slab, the Bloch–Floquet expression is valid and can well define the solution since the limited numbers of harmonic components are excited for a finite length of propagation [43].

The fields in the space-time modulated slab can be expressed as the superposition of all allowed modes taking the form of Bloch–Floquet expansion,

$$E_z(x,t) = \sum_{p,\,m,\,n=-\infty}^{+\infty} a_p E_{m,n}^{(p)} e^{ik_m^{(p)}(x+L_m/2) - i\omega_{m,n} t}, \tag{A4a}$$

$$H_z(x,t) = \sum_{p,\,m,\,n=-\infty}^{+\infty} a_p H_{m,n}^{(p)} e^{ik_m^{(p)}(x+L_m/2) - i\omega_{m,n} t}, \tag{A4b}$$

for $x \in [-L_m/2, L_m/2]$, where a_p represents the unknown modal coefficient of mode p, and k_p and $[E_{m,n}^{(p)}, H_{m,n}^{(p)}]^T$ are the

eigenvalue and the eigenstate of mode p solved by Eq. (A3). At the boundary between the background media and the space-time modulated slab, the electric and magnetic fields should be continuous at any time. It gives

$$E_z\left(x=\pm\frac{L}{2}+0^+,t;\omega_{m,n}\right)=E_z\left(x=\pm\frac{L}{2}+0^-,t;\omega_{m,n}\right), \tag{A5a}$$

$$H_y\left(x=\pm\frac{L}{2}+0^+,t;\omega_{m,n}\right)=H_y\left(x=\pm\frac{L}{2}+0^-,t;\omega_{m,n}\right). \tag{A5b}$$

The reflection and transmission fields contain all harmonic components

$$E_z^r(x,t)=\sum_{m,\,n=-\infty}^{+\infty}E_{m,n}^r e^{-i\omega_{m,n}[(x+L/2)/v_s+t]}, \tag{A6a}$$

$$H_z^r(x,t)=\sum_{m,\,n=-\infty}^{+\infty}\eta_s E_{m,n}^r e^{-i\omega_{m,n}[(x+L/2)/v_s+t]}, \tag{A6b}$$

$$E_z^t(x,t)=\sum_{m,\,n=-\infty}^{+\infty}E_{m,n}^t e^{i\omega_{m,n}[(x-L/2)/v_s-t]}, \tag{A6c}$$

$$H_z^t(x,t)=\sum_{m,\,n=-\infty}^{+\infty}-\eta_s E_{m,n}^t e^{i\omega_{m,n}[(x-L/2)/v_s-t]}, \tag{A6d}$$

where $\eta_s=(\varepsilon_s/\mu_0)^{1/2}$ represents the admittance of the background media. Note that the reflection and the transmission waves should satisfy the dispersion relation $\omega/v_s=k$. For a given complex frequency, the corresponding wavenumber will be a complex number, and the amplitude of waves will decay with propagation and be amplified with time.

By applying boundary conditions, the scattering coefficients can be solved. In practical calculation, the harmonic order is truncated. For the convenience of calculation, the boundary conditions are rewritten in matrix form

$$\begin{bmatrix}\mathbf{E}(x=-L/2+0^-;\omega_{m,n})\\ \mathbf{H}(x=-L/2+0^-;\omega_{m,n})\end{bmatrix}=\mathbf{T}_i\begin{bmatrix}\mathbf{E}_i\\ \mathbf{E}_r\end{bmatrix}, \tag{A7a}$$

$$\begin{bmatrix}\mathbf{E}(x;\omega_{m,n})\\ \mathbf{H}(x;\omega_{m,n})\end{bmatrix}=\mathbf{T}_p(x)\mathbf{a}_p \text{ for } x=\pm\frac{L}{2}+0^{\mp}, \tag{A7b}$$

$$\begin{bmatrix}\mathbf{E}(x=L/2+0^+;\omega_{m,n})\\ \mathbf{H}(x=L/2+0^+;\omega_{m,n})\end{bmatrix}=\mathbf{T}_t\begin{bmatrix}\mathbf{E}_t\\ \mathbf{O}\end{bmatrix}, \tag{A7c}$$

where $\mathbf{E}_{i,(r,t)}$ is a column vector composed of all harmonic fields; the transfer matrix of the incident and transmission media is $\mathbf{T}_i=\mathbf{T}_t=\begin{bmatrix}\mathbf{I} & \mathbf{I}\\ -\eta_s\mathbf{I} & \eta_s\mathbf{I}\end{bmatrix}$ and the transfer matrix in the space-time modulated media $\mathbf{T}_p(x)=$

$$\begin{bmatrix}
\vdots & \vdots & \\
\cdots & E_{m-1,n}^{(p-1)}e^{ik_{p-1,m-1}(x+L/2)} & E_{m-1,n}^{(p)}e^{ik_{p,m-1}(x+L/2)} & \cdots\\
\cdots & E_{m,n}^{(p-1)}e^{ik_{p-1,m}(x+\frac{L}{2})} & E_{m,n}^{(p)}e^{ik_{p,m}(x+L/2)} & \cdots\\
\vdots & \vdots & \\
\cdots & H_{m-1,n}^{(p-1)}e^{ik_{p-1,m-1}(x+L/2)} & H_{m-1,n}^{(p)}e^{ik_{p,m-1}(x+L/2)} & \cdots\\
\cdots & H_{m,n}^{(p-1)}e^{ik_{p-1,m}(x+L/2)} & H_{m,n}^{(p)}e^{ik_{p,m}(x+L/2)} & \cdots\\
\vdots & \vdots &
\end{bmatrix}$$

are written according to Eqs. (A6) and (A4), respectively.

By eliminating the modal coefficients $\mathbf{a}_p$, it gives

$$\begin{bmatrix}\mathbf{E}_t\\ \mathbf{O}\end{bmatrix}=\mathbf{T}\begin{bmatrix}\mathbf{E}_i\\ \mathbf{E}_r\end{bmatrix}=\begin{bmatrix}\mathbf{T}_{11} & \mathbf{T}_{12}\\ \mathbf{T}_{21} & \mathbf{T}_{22}\end{bmatrix}\begin{bmatrix}\mathbf{E}_i\\ \mathbf{E}_r\end{bmatrix}, \tag{A8}$$

where the transfer matrix $\mathbf{T}=\mathbf{T}_t^{-1}\mathbf{T}_p(x=\frac{L}{2})\mathbf{T}_p^{-1}(x=-\frac{L}{2})\mathbf{T}_i$.

Hence, the scattering coefficients can be solved by

$$\begin{cases}\mathbf{E}_r=-\mathbf{T}_{22}^{-1}\mathbf{T}_{21}\mathbf{E}_i\\ \mathbf{E}_t=\mathbf{T}_{11}\mathbf{E}_i+\mathbf{T}_{12}\mathbf{E}_r\end{cases}. \tag{A9}$$

Equations (A8) and (A9) are available for static solutions with real frequency. However, the system is unstable if the modulation length is larger than the threshold length and the frequency will be a complex number (see Fig. 4). In this case, the amplitude of the reflection and the transmission fields will increase with time. However, for the static input with constant amplitude, the boundary conditions cannot be satisfied. In fact, since the lasing state corresponds to a singular state of the space-time modulated system, the scattering fields can be solved by the eigenvalue problem without incidence. Then, Eq. (A8) can be rewritten as

$$\begin{bmatrix}\mathbf{T}_{12} & -\mathbf{I}\\ \mathbf{T}_{22} & \mathbf{O}\end{bmatrix}\begin{bmatrix}\mathbf{E}_r\\ \mathbf{E}_t\end{bmatrix}=\mathbf{M}\begin{bmatrix}\mathbf{E}_r\\ \mathbf{E}_t\end{bmatrix}=\mathbf{O}. \tag{A10}$$

Note that this eigenvalue problem is quite different from the common scattering problem. For common scattering problems, e.g., Eq. (A8), the transfer matrix $\mathbf{T}_p$ can be explicitly expressed by solving Eq. (A3) for a given incident frequency. However, for the unstable state, the frequency for lasing is an unsolved singularity of Eq. (A10), and the transfer matrix $\mathbf{T}_p$ cannot be explicitly expressed. Therefore, to solve this eigenvalue problem, Eq. (A3) needs to be involved at the same time. We solve it by first giving trial solutions of the eigenfrequency. Hence, the wavenumber k_p and the corresponding eigenvectors can be explicitly expressed by Eq. (A3). In general, the eigenfrequency for lasing can be solved by finding the zero determinant of matrix $\mathbf{M}$.

APPENDIX B: PA IN A TIME-FLOQUET SLAB

In this section, following the same procedure in Ref. [50], we calculate the lasing threshold of the time-varying slab with permittivity

$$\varepsilon(x,t)=\varepsilon_s(1+2\alpha\cos\Omega t). \tag{B1}$$

In the meantime, time modulation plays a role in the PA of the fundamental mode in Eq. (1). A similar dependency of the exponential growth rate on the modulation length, as shown in Figs. 4(a) and 5(c), is also presented in this section.

Due to the periodicity of permittivity, the solution of Maxwell's equations [Eqs. (A1a) and (A1b)] can be expanded as the time-Floquet form. For small α, only the harmonic modes at the frequencies near $\pm\Omega/2$ have non-negligible amplitude. Hence, the ansatz can be expressed as

$$E_z(x,t) = e^{ikx-i\omega t}(E_{-1}e^{i\Omega t} + E_0). \tag{B2}$$

By inserting Eqs. (B1) and (B2) into Maxwell's equations, the eigenvalues and the eigenstates can be solved. Here, we introduce dimensionless parameters $\kappa = v_s k/(\Omega/2) = 1 + \delta\kappa$ and $\tilde{\omega} = \omega/(\Omega/2) = 1 + \delta\tilde{\omega}$ and apply approximation $\delta\kappa^2 \approx 0$, $\delta\tilde{\omega}^2 \approx 0$, and $\omega^2 \approx (\Omega/2)^2$. The dispersion relation and eigenstates of the time-varying media can be explicitly expressed as

$$\delta\kappa^2 - \delta\tilde{\omega}^2 \approx (\alpha/2)^2, \tag{B3a}$$

$$\begin{bmatrix} E_0 \\ E_{-1} \end{bmatrix} = \begin{bmatrix} 1 \\ \frac{\delta\kappa-\delta\tilde{\omega}}{\alpha/2} \end{bmatrix}. \tag{B3b}$$

The dispersion relations are shown in Figs. 8(a) and 8(b).

Next, we solve the transition point from stable state to lasing state. For real values of $\delta\tilde{\omega} = \pm\Delta$, it gives real values of $\delta\kappa = \pm[(\alpha/2)^2 + \Delta^2]^{1/2} = \pm\gamma$, where γ, $\Delta \geq 0$. By setting $E_0^{(0)} = E_0^{(1)} = 1$, it gives $E_{-1}^{(0)} = (\gamma - \Delta)/(\alpha/2) = c$ and $E_{-1}^{(1)} = -(\gamma - \Delta)/(\alpha/2) = -c$. Assuming a plane wave incident from the left ($x < 0$), the field inside the slab should contain all possible harmonic components. The expression of the electric fields can be found as

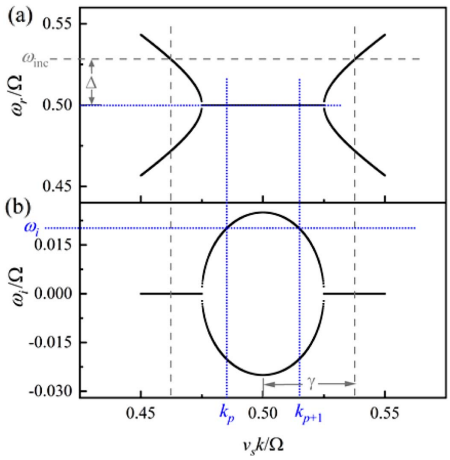

Fig. 8. Dispersion curve of the time-Floquet media with permittivity $\varepsilon(t) = \varepsilon_s(1 + 2\alpha\cos\Omega t)$. (a) The real part and (b) the imaginary part of the eigenfrequency are shown.

To excite the lasing state, a phase condition needs to be satisfied [50]. When the length of modulation L_m is smaller than the threshold length l_{PA}, this phase condition cannot be fulfilled. For $L_m > l_{PA}$, the lasing state can be excited with a complex eigenfrequency.

Here, we use the Bloch–Floquet theory in Appendix A to analytically solve the eigenfrequency with $\alpha = 0$ and $m = 0$. Note that the imaginary part of frequency ω_i is unknown.

$$E_z(x,t) = \begin{cases} e^{-i(1+\Delta)\frac{\Omega}{2}(t-xv_s^{-1})} + r_0 e^{-i(1+\Delta)\frac{\Omega}{2}(t+xv_s^{-1})} + r_{-1}e^{i(1-\Delta)\frac{\Omega}{2}(t+xv_s^{-1})}, x \leq 0 \\ e^{-i(1+\Delta)\frac{\Omega}{2}t}[Ae^{i(1+\gamma)\frac{\Omega}{2}xv_s^{-1}} + Be^{-i(1+\gamma)\frac{\Omega}{2}xv_s^{-1}} - C^*ce^{-i(1-\gamma)\frac{\Omega}{2}xv_s^{-1}} - D^*ce^{i(1-\gamma)\frac{\Omega}{2}xv_s^{-1}}] \\ + e^{i(1-\Delta)\frac{\Omega}{2}t}[Ace^{i(1+\gamma)\frac{\Omega}{2}xv_s^{-1}} + Bce^{-i(1+\gamma)\frac{\Omega}{2}xv_s^{-1}} + C^*e^{-i(1-\gamma)\frac{\Omega}{2}xv_s^{-1}} + D^*e^{i(1-\gamma)\frac{\Omega}{2}xv_s^{-1}}], x \in [0, L] \\ t_0 e^{-i(1+\Delta)\frac{\Omega}{2}[t-(x-L)v_s^{-1}]} + t_{-1}e^{i(1-\Delta)\frac{\Omega}{2}[t-(x-L)v_s^{-1}]}, x \geq L \end{cases}. \tag{B4}$$

By applying the boundary conditions at $x = 0$, L, i.e., the continuity of electric fields and the derivative of electric fields for x at each harmonic frequency, note that to simplify the calculation, the approximations of $1 + \Delta \approx 1$ and $1 + \gamma \approx 1$ are applied in derivation. The reflection and transmission coefficients can be analytically solved:

$$r = r_0 + r_{-1} = -i\tan(\alpha KL/4). \tag{B5a}$$

$$t = t_0 + t_{-1} = \frac{\exp(iKL/2)}{\cos(\alpha KL/4)}. \tag{B5b}$$

For more details on the solving processes, please refer to Ref. [51]. The scattering coefficients r and t will tend to infinity when $\alpha KL/4 = \pi/2$, as shown in Fig. 9(a). Hence, the threshold length of lasing $l_{PA} = 2\pi/(\alpha K) = v_s\pi/(\alpha\Omega/2)$. When the modulation length is equal to the threshold length, the amplitude of the reflection and the transmission waves will linearly increase with time, as shown in Fig. 9(b).

In the meantime, as shown in Fig. 8(b), the wavenumbers, i.e., k_p and k_{p-1}, are related to frequency through dispersion relation. Therefore, to solve the lasing state, Eqs. (A3) and (A10) should be solved at the same time.

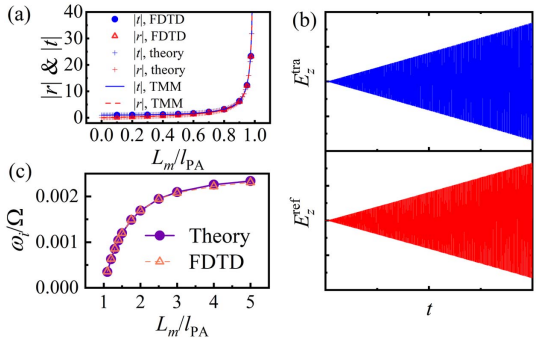

Fig. 9. (a) Dependence of the amplitude of the reflection and the transmission coefficients on the modulation length L_m. (b) The reflection and transmission fields for $L_m = l_{PA}$. (c) The imaginary part of the eigenfrequency as the modulation length increases for $L_m > l_{PA}$. Here, $\alpha = 0.01$.

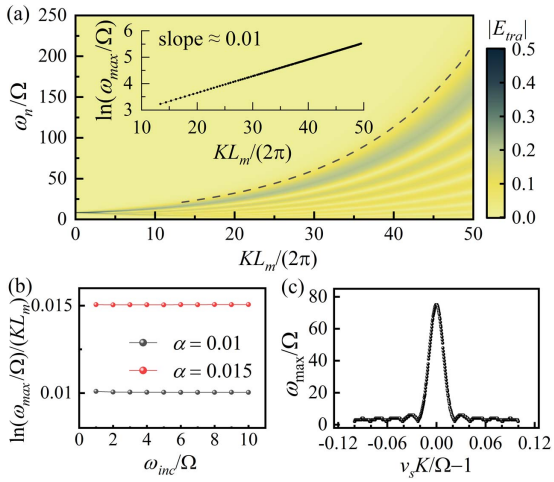

Fig. 10. (a) The frequency up-conversion effect of the LA and the characterization of the luminal gain. (b) The luminal gain with varying excitation frequencies and modulation strengths. (c) The relationship between the highest order of frequency conversion and phase mismatching.

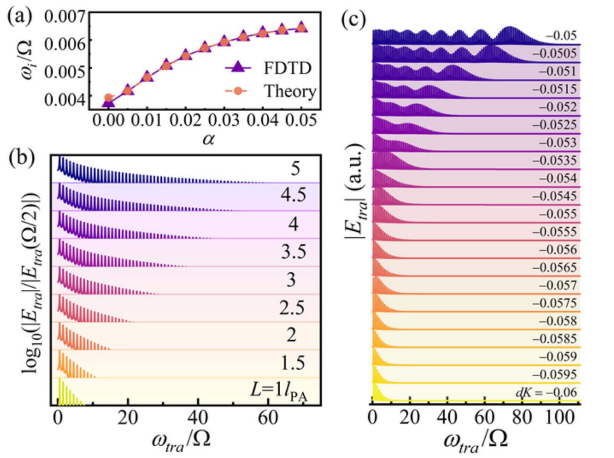

Fig. 11. (a) The exponential growth rate of the cascaded PA as modulation strength α increases. (b) The number of harmonic components in the cascaded PA as the modulation length increases. Here, $\alpha = 0.02$ and $\beta = 0.1$. (c) The dependence of the cascaded PA on phase mismatching $dK = K/K_s - 1$.

As shown in Fig. 9(c), the parametric gain of the time-varying slab increases with the modulation length since less energy in the slab is lost due to scattering.

APPENDIX C: THE FREQUENCY CONVERSION IN LA

In this section, we show the LA supported by media with permittivity $\varepsilon(x,t) = \varepsilon_s[1 + 2\alpha\cos(Kx - \Omega t)]$ and the modulation velocity $v_m = v_s$. As shown in Fig. 10(a), we depict the amplitude of the electric fields transmitted from the space-time modulated slab. The highest order of frequency conversion is selected at which the amplitude equals 10^{-2} [the dashed line in Fig. 10(a)]. The corresponding frequency is denoted as $\omega_{\max}$. The exponential growth relation between $\omega_{\max}$ and the modulation length is verified in the inset of Fig. 10(a).

This exponential relationship does not change with the varying incident frequencies and modulation strengths, as shown in Fig. 10(b). Therefore, the luminal gain can be defined as $\ln(\omega_{\max}/\Omega)/(KL_m)$. It is found that the value of luminal gain is just equal to the modulation strength α.

Another result showing the parametric nature of LA is that the relation between frequency up-conversion effect and phase mismatching $K - \Omega/v_s$ has a sinc function shape, as shown in Fig. 10(c).

APPENDIX D: LUMINAL GAIN AND PARAMETRIC GAIN IN CASCADED PA

As shown in Fig. 11(a), the introduction of luminal modulation does not undermine the parametric gain. The parametric gain is improved with the increased total modulation strength.

In Fig. 11(b), the highest harmonic frequency for amplification $\omega_{\max}$ increases with the modulation length, but they do not follow an exponential growth relationship as the LA shown in Appendix C. The luminal gain in cascaded PA represents the capability to transfer energy from the amplifying fundamental mode to the high harmonic components. It is essentially different from the luminal gain described above.

We also show the influence of modulation velocity on cascaded PA [Fig. 11(c)]. It is found that the high harmonic components can be efficiently amplified for a small deviation of v_m from v_s. In the meantime, the excitation of harmonic components in cascaded PA can be manipulated by this deviation.

APPENDIX E: DESIGN OF PHOTONIC BANDSTRUCTURE FOR CPO

To reduce the threshold length of lasing, the photonic crystal (PC) is designed to forbid the propagation of light at each harmonic frequency, as shown in Fig. 12(a). The photonic crystal is composed of alternative dielectric layers with a refractive index $n_a = 3.5$ and $n_b = 1$. All harmonic frequencies are just located at the center of the bandgap. This special case happens when the thicknesses of dielectric a and b satisfy $d_a = n_b\Lambda/(n_a + n_b)$ and $d_b = n_a\Lambda/(n_a + n_b)$, where Λ is the period of photonic crystals. The bandgaps are closed at frequencies $m\Omega$ for $m \in Z$.

The resonant condition of the cavity is reached if the phase change of light propagating a round trip in a cavity is $\Phi = 2k_aL + \Phi_L + \Phi_R = 2m\pi$ for $m \in Z$, where $\Phi_L\,(\Phi_R)$ is the reflection phase of the right (left) PCs incident from the cavity. At the center of bandgaps in Fig. 12(a), the reflection phase of photonic crystals is just equal to π. Hence, the resonant condition is satisfied at all harmonic frequencies if the length of cavity $L_m = m\pi v_s/\omega$ or $L_m = m\alpha l_{\mathrm{PA}}$ for $m \in Z$. The phase change Φ is given in Fig. 12(b).

We also design the CPO operating at a single frequency. The corresponding bandstructure is shown in Fig. 12(c). The bandgap exists at all harmonic frequencies except for the harmonic frequency of 10.5Ω.

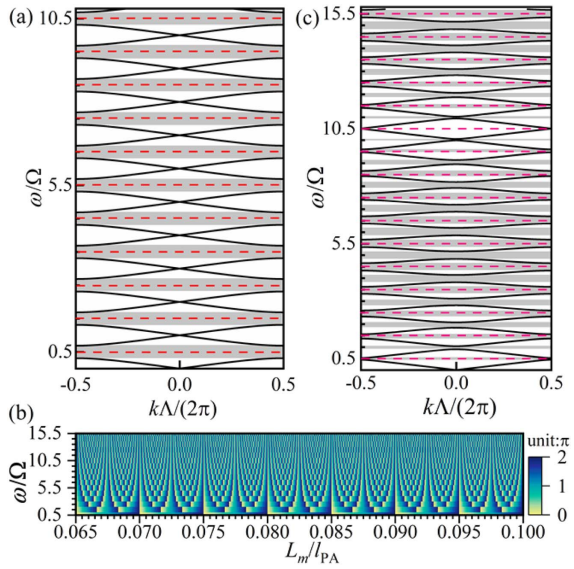

Fig. 12. (a) The bandstructure of photonic crystals in Fig. 5(b). (b) The phase change of light propagating one round trip in the cavity. The cavity is resonant when this phase shift equals 2π. Here, $\Lambda = 0.6429(2\pi c_0/\Omega)$, $d_a = n_b\Lambda/(n_a + n_b)$, and $d_b = n_a\Lambda/(n_a + n_b)$. (c) The bandstructure of photonic crystals in Figs. 5(c) and 5(d). Here, $\Lambda = 0.3197(2\pi c_0/\Omega)$, $d_a = 0.8502\Lambda$, and $d_b = 0.1498\Lambda$.

Funding. Agency for Science, Technology and Research (A18A7b0058, A20E5c0095); Singapore Ministry of Education (MOE2018-T2-2-189(S)); National Research Foundation Singapore Competitive Research Program (NRF-CRP22-2019-0006, NRF-CRP23-2019-0007); National Natural Science Foundation of China (62120106001); Priority Academic Program Development (PAPD) of the Jiangsu Higher Education Institution.

Acknowledgment. Q. Y. and Y. L. conceived the original idea. Q. Y. performed the numerical and analytical calculations, and all authors discussed the results and commented on the analyses. Q. Y. wrote the manuscript, and all authors provided feedback.

Disclosures. The authors declare no competing interest.

Data Availability. Data underlying the results presented in this paper are not publicly available at this time but may be obtained from the authors upon reasonable request.

REFERENCES

1. A. M. Shaltout, M. Clerici, N. Kinsey, R. Kaipurath, J. Kim, E. G. Carnemolla, D. Faccio, A. Boltasseva, V. M. Shalaev, and M. Ferrera, "Doppler-shift emulation using highly time-refracting TCO layer," in *Conference on Lasers and Electro-Optics (CLEO)* (2016), pp. 1–2.
2. N. Karl, P. P. Vabishchevich, M. R. Shcherbakov, S. Liu, M. B. Sinclair, G. Shvets, and I. Brener, "Frequency conversion in a time-variant dielectric metasurface," Nano Lett. **20**, 7052–7058 (2020).
3. K. Lee, J. Son, J. Park, B. Kang, W. Jeon, F. Rotermund, and B. Min, "Linear frequency conversion via sudden merging of meta-atoms in time-variant metasurfaces," Nat. Photonics **12**, 765–773 (2018).
4. Z. Liu, Z. Li, and K. Aydin, "Time-varying metasurfaces based on graphene microribbon arrays," ACS Photon. **3**, 2035–2039 (2016).
5. X. Wen, X. Zhu, A. Fan, W. Y. Tam, J. Zhu, H. W. Wu, F. Lemoult, M. Fink, and J. Li, "Unidirectional amplification with acoustic non-Hermitian space–time varying metamaterial," Commun. Phys. **5**, 18 (2022).
6. T. T. Koutserimpas, A. Alù, and R. Fleury, "Parametric amplification and bidirectional invisibility in PT-symmetric time-Floquet systems," Phys. Rev. A **97**, 013839 (2018).
7. S. Lee, J. Park, H. Cho, Y. Wang, B. Kim, C. Daraio, and B. Min, "Parametric oscillation of electromagnetic waves in momentum band gaps of a spatiotemporal crystal," Photon. Res. **9**, 142–150 (2021).
8. H. Lira, Z. Yu, S. Fan, and M. Lipson, "Electrically driven nonreciprocity induced by interband photonic transition on a silicon chip," Phys. Rev. Lett. **109**, 033901 (2012).
9. E. A. Kittlaus, N. T. Otterstrom, P. Kharel, S. Gertler, and P. T. Rakich, "Non-reciprocal interband Brillouin modulation," Nat. Photonics **12**, 613–619 (2018).
10. X. Guo, Y. Ding, Y. Duan, and X. Ni, "Nonreciprocal metasurface with space-time phase modulation," Light Sci. Appl. **8**, 123 (2019).
11. D.-W. Wang, H.-T. Zhou, M.-J. Guo, J.-X. Zhang, J. Evers, and S.-Y. Zhu, "Optical diode made from a moving photonic crystal," Phys. Rev. Lett. **110**, 093901 (2013).
12. S. A. Horsley, J.-H. Wu, M. Artoni, and G. C. La Rocca, "Optical nonreciprocity of cold atom Bragg mirrors in motion," Phys. Rev. Lett. **110**, 223602 (2013).
13. M. S. Kang, A. Butsch, and P. St. J. Russell, "Reconfigurable light-driven opto-acoustic isolators in photonic crystal fibre," Nat. Photonics **5**, 549–553 (2011).
14. X. Wang, G. Ptitcyn, V. S. Asadchy, A. Díaz-Rubio, M. S. Mirmoosa, S. Fan, and S. A. Tretyakov, "Nonreciprocity in bianisotropic systems with uniform time modulation," Phys. Rev. Lett. **125**, 266102 (2020).
15. J. Wang, J. F. Herrmann, J. D. Witmer, A. H. Safavi-Naeini, and S. Fan, "Photonic modal circulator using temporal refractive-index modulation with spatial inversion symmetry," Phys. Rev. Lett. **126**, 193901 (2021).
16. A. M. Shaltout, V. M. Shalaev, and M. L. Brongersma, "Spatiotemporal light control with active metasurfaces," Science **364**, eaat3100 (2019).
17. E. Galiffi, R. Tirole, S. Yin, H. Li, S. Vezzoli, P. A. Huidobro, M. G. Silveirinha, R. Sapienza, A. Alù, and J. B. Pendry, "Photonics of time-varying media," Adv. Photon. **4**, 014002 (2022).
18. J. N. Winn, S. Fan, J. D. Joannopoulos, and E. P. Ippen, "Interband transitions in photonic crystals," Phys. Rev. B **59**, 1551–1554 (1999).
19. A. Bahabad, M. M. Murnane, and H. C. Kapteyn, "Quasi-phase-matching of momentum and energy in nonlinear optical processes," Nat. Photonics **4**, 570–575 (2010).
20. A. Y. Song, Y. Shi, Q. Lin, and S. Fan, "Direction-dependent parity-time phase transition and nonreciprocal amplification with dynamic gain-loss modulation," Phys. Rev. A **99**, 013824 (2019).
21. N. Chamanara, Z.-L. Deck-Léger, C. Caloz, and D. Kalluri, "Unusual electromagnetic modes in space-time-modulated dispersion-engineered media," Phys. Rev. A **97**, 063829 (2018).
22. H. Li, H. Moussa, D. Sounas, and A. Alù, "Parity-time symmetry based on time modulation," Phys. Rev. Appl. **14**, 031002 (2020).
23. P. A. Huidobro, E. Galiffi, S. Guenneau, R. V. Craster, and J. B. Pendry, "Fresnel drag in space-time-modulated metamaterials," Proc. Natl. Acad. Sci. USA **116**, 24943–24948 (2019).
24. Y. Sharabi, E. Lustig, and M. Segev, "Disordered photonic time crystals," Phys. Rev. Lett. **126**, 163902 (2021).
25. E. Galiffi, Y.-T. Wang, Z. Lim, J. B. Pendry, A. Alù, and P. A. Huidobro, "Wood anomalies and surface-wave excitation with a time grating," Phys. Rev. Lett. **125**, 127403 (2020).
26. K. Wang, A. Dutt, K. Y. Yang, C. C. Wojcik, J. Vučković, and S. Fan, "Generating arbitrary topological windings of a non-Hermitian band," Science **371**, 1240–1245 (2021).

27. A. Dutt, M. Minkov, I. A. D. Williamson, and S. Fan, "Higher-order topological insulators in synthetic dimensions," Light Sci. Appl. **9**, 131 (2020).
28. Q. Lin, M. Xiao, L. Yuan, and S. Fan, "Photonic Weyl point in a two-dimensional resonator lattice with a synthetic frequency dimension," Nat. Commun. **7**, 13731 (2016).
29. A. Dutt, Q. Lin, L. Yuan, M. Minkov, M. Xiao, and S. Fan, "A single photonic cavity with two independent physical synthetic dimensions," Science **367**, 59–64 (2020).
30. L. Yuan, Q. Lin, M. Xiao, and S. Fan, "Synthetic dimension in photonics," Optica **5**, 1396–1405 (2018).
31. N. Kinsey, C. DeVault, J. Kim, M. Ferrera, V. M. Shalaev, and A. Boltasseva, "Epsilon-near-zero Al-doped ZnO for ultrafast switching at telecom wavelengths," Optica **2**, 616–622 (2015).
32. Y. Wang, B. Yousefzadeh, H. Chen, H. Nassar, G. Huang, and C. Daraio, "Observation of nonreciprocal wave propagation in a dynamic phononic lattice," Phys. Rev. Lett. **121**, 194301 (2018).
33. T. Kang, B. Fan, J. Qin, W. Yang, S. Xia, Z. Peng, B. Liu, S. Peng, X. Liang, T. Tang, L. Deng, Y. Luo, H. Wang, Q. Zhou, and L. Bi, "Mid-infrared active metasurface based on Si/VO_2 hybrid meta-atoms," Photon. Res. **10**, 373–380 (2022).
34. S.-Q. Li, X. Xu, R. Maruthiyodan Veetil, V. Valuckas, and R. Paniagua-Domínguez, "Phase-only transmissive spatial light modulator based on tunable dielectric metasurface," Science **364**, 1087–1090 (2019).
35. K. Midorikawa, "Progress on table-top isolated attosecond light sources," Nat. Photonics **16**, 267–278 (2022).
36. L. Ledezma, R. Sekine, Q. Guo, R. Nehra, S. Jahani, and A. Marandi, "Intense optical parametric amplification in dispersion-engineered nanophotonic lithium niobate waveguides," Optica **9**, 303–308 (2022).
37. P. A. Andrekson and M. Karlsson, "Fiber-based phase-sensitive optical amplifiers and their applications," Adv. Opt. Photon. **12**, 367–428 (2020).
38. C. M. Caves, "Quantum limits on noise in linear amplifiers," Phys. Rev. D **26**, 1817–1839 (1982).
39. J. A. Levenson, I. Abram, Th. Rivera, and Ph. Grangier, "Reduction of quantum noise in optical parametric amplification," J. Opt. Soc. Am. B **10**, 2233–2238 (1993).
40. A. Cullen, "A travelling-wave parametric amplifier," Nature **181**, 332 (1958).
41. P. K. Tien, "Parametric amplification and frequency mixing in propagating circuits," J. Appl. Phys. **29**, 1347–1357 (1958).
42. E. S. Cassedy and A. A. Oliner, "Dispersion relations in time-space periodic media: Part I—stable interactions," Proc. IEEE **51**, 1342–1359 (1963).
43. E. Galiffi, P. A. Huidobro, and J. B. Pendry, "Broadband nonreciprocal amplification in luminal metamaterials," Phys. Rev. Lett. **123**, 206101 (2019).
44. E. S. Cassedy, "Dispersion relations in time-space periodic media part II—Unstable interactions," Proc. IEEE **55**, 1154–1168 (1967).
45. Y. Zou, S. Chakravarty, C.-J. Chung, X. Xu, and R. T. Chen, "Mid-infrared silicon photonic waveguides and devices [Invited]," Photon. Res. **6**, 254–276 (2018).
46. X. Lin, H. Hu, S. Easo, Y. Yang, Y. Shen, K. Yin, M. P. Blago, I. Kaminer, B. Zhang, H. Chen, J. Joannopoulos, and M. Soljacic, "A Brewster route to Cherenkov detectors," Nat. Commun. **12**, 5554 (2021).
47. H. Hu, X. Lin, D. Liu, H. Chen, B. Zhang, and Y. Luo, "Broadband enhancement of Cherenkov radiation using dispersionless plasmons," Adv. Sci. **9**, 2200538 (2022).
48. N. Rivera and I. Kaminer, "Light–matter interactions with photonic quasiparticles," Nat. Rev. Phys. **2**, 538–561 (2020).
49. H. Hu, X. Lin, L. J. Wong, Q. Yang, D. Liu, B. Zhang, and Y. Luo, "Surface Dyakonov–Cherenkov radiation," eLight **2**, 2 (2022).
50. D. Holberg and K. Kunz, "Parametric properties of fields in a slab of time-varying permittivity," IEEE Trans. Antennas Propag. **14**, 183–194 (1966).
51. D. E. Holberg, *Electromagnetic Wave Propagation in Media of Periodically Time-Varying Permittivity* (Sandia Corporation, 1965).